

Super-Arrhenius diffusion in a binary colloidal mixture at low volume fraction: An effect of depletion interaction due to an asymmetric barrier

Jalim Singh, Mahammad Mustakim, and A. V. Anil Kumar*

School of Physical Sciences, National Institute of Science Education and Research, HBNI, Jatni, Bhubaneswar 752050, India.

(Dated: January 26, 2021)

We report results from the molecular dynamics simulations of a binary colloidal mixture subjected to an external potential barrier along one of the spatial directions at low volume fraction, $\phi = 0.2$. The variations in the asymmetry of the external potential barrier do not change the dynamics of the smaller particles, showing Arrhenius diffusion. However, the dynamics of the larger particles shows a crossover from sub-Arrhenius to super-Arrhenius diffusion with the asymmetry in the external potential at the low temperatures and low volume fraction. Super-Arrhenius diffusion is generally observed in the high density systems where the transient cages are present due to dense packing, e.g., supercooled liquids, jammed systems, diffusion through porous membranes, dynamics within the cellular environment, etc. This model can be applied to study the molecular transport across cell membranes, nano-, and micro-channels which are characterized by spatially asymmetric potentials.

I. INTRODUCTION

Binary colloidal mixtures of unequal sizes serve as a paradigm for entropic manipulation of structural as well as dynamical properties of soft matter [1–5]. The primary reason behind this is the attractive depletion interaction between the larger species of the mixture due to the presence of the smaller species. The physical interpretation of depletion interactions is that there exists an effective attractive interaction between the larger particles which favors the overlap of depletion layers around them thereby providing a larger free volume available for the smaller particles [6]. This interpretation hinges on the view that an osmotic pressure imbalance pushes two larger particles close to each other when they reach within a length scale set by the smaller particles. It was first proposed by Asakura and Oosawa [7] and later reconsidered by Vrij [8] while explaining the phase behavior of colloid-polymer mixtures. Depletion interactions are invoked to explain a large variety of phenomena in mixtures such as colloidal crystallization [9–12], vitrification of colloids [13–17], dynamics in crowded medium [18–20], etc.

It has been shown that in a binary colloidal mixture subjected to external potentials (symmetric barrier at the middle and confinement along the z -direction), there exists depletion interaction not only between the larger particles but also between the external potentials and the larger particles [21]. When the external potential is finite, this depletion interaction alters structural and dynamical properties significantly. When a binary mixture of colloids is subjected to an external repulsive potential barrier, the depletion interaction between the repulsive barrier and the larger particles leads to a demixing in the mixture [21, 22]. Moreover, dynamical properties of both sizes of particles in the mixture deviate substantially in the presence of the external barrier (without the confining potential) and show a lot of interesting phenom-

ena [23]. For example, at low temperatures, the smaller particles get localized between the external potential barriers leading to a slowing down in their dynamics, similar to the dynamics of supercooled liquids [23]. This slowing down is manifested by a plateau in the mean-squared displacement at intermediate times, non-zero non-Gaussian parameter, two-step relaxation in the self-intermediate scattering function, etc. This is intriguing as this occurs even at a very low volume fraction. However, the larger particles do not get localized between the barriers and continue to show normal diffusion even at low temperatures. This is attributed to the reduction in effective potential barrier the larger particles have to cross during their dynamics due to the depletion interaction. At high temperatures, the smaller particles diffuse faster than the larger particles, which is expected. However, as temperature decreases, the larger particles start diffusing faster than their smaller counterparts, thus showing a crossover in the diffusion coefficients. This occurs because the diffusion coefficient of the larger components (D_l) decreases very slowly with decreasing temperature. This weak dependence of D_l on temperature suggests that the diffusion of the larger components is no longer Arrhenius and the activation energy for diffusion is temperature dependent. It has been shown that the larger particles' diffusion is sub-Arrhenius and activation energy decreases with temperature whereas the diffusion of the smaller particles is Arrhenius with a constant activation energy [24]. In general, sub-Arrhenius diffusion is considered to be intimately related to quantum phenomena and has been observed mostly in systems where quantum tunneling plays an important role such as in certain chemical reactions [25, 26]. In fact, the binary colloidal mixture, subjected to an external Gaussian potential barrier, is the first classical system which has been observed to undergo sub-Arrhenius diffusion [24].

It is shown that an asymmetry of cell-membrane channel controls the transport across it by ratchet like mechanism, when non-equilibrium fluctuations are present [27]. Interestingly, Kolomeisky shows that asymmetry in the external potential alters the molecular transport across

* anil@niser.ac.in

cell membrane, even without nonequilibrium fluctuations [28]. This results in the asymmetric diffusion across such membrane channels in which particles' diffusion dominates in one direction [29]. It is interesting to study dynamical properties associated with this anomalous diffusion. Here, we investigate the effect of *asymmetry* in the external potential barrier on the structure and dynamics of the binary colloidal mixture, compared to Refs. [21, 23] where the external potential barrier is *symmetric*, using canonical ensemble molecular dynamics simulations. We find that as the asymmetry in the external potential increases, the diffusion of the larger particles changes from sub-Arrhenius to super-Arrhenius. This happens due to the crowding of the larger particles near the barrier. This crowding is more on the steeper side of the potential when its asymmetry becomes large. A theoretical and experimental study on colloidal particles at low volume fractions by Dalle-Ferrier *et al.* also shows the dynamical signatures of supercooled liquids in the system due to external sinusoidal potentials [30]. Interestingly, by calculating the self part of the van-Hove correlation function of small and large particles, along the applied external potential, we reveal that the transport of the particles is bidirectional. Thorn *et al.* show the asymmetrical optical trapping of particles using two laser beams in which one laser beam produces the external potential such that atoms transmit to the other side, whereas the other laser beam represents a reflecting potential, thus demonstrate the unidirectional atomic motion [31]. Our model can be realized in such experiments where the external potential remains asymmetric while maintaining bidirectional transport.

The remainder of this paper is organized as follows: we begin with a description of our model and the simulation details in Sec. II. The dynamical properties as well as the structural changes associated with the asymmetric potential are presented in Sec. III. Finally, we conclude our results in Sec. IV.

II. MODEL

We perform constant NVT molecular dynamics simulations of a equi-volume colloidal mixture consisting of two different sizes of particles with equal masses. The inter-particle interactions in the colloidal mixture are soft and purely repulsive, which are given by the potential

$$V(r_{ij}) = \epsilon_{ij} \left(\frac{\sigma_{ij}}{r_{ij}} \right)^{12}, \quad (1)$$

where $(i, j) \in (s, l)$ are corresponding to the small and large size particles. The simulation parameters are: $\sigma_{ss} = 1.0$, $\sigma_{ll} = 2.0$, $\epsilon_{ss} = 1.0$, and $\epsilon_{ll} = 4.0$ [24]. Cross interaction parameters are obtained using Lorentz-Berthelot additive mixture rules, i.e., $\sigma_{sl} = (\sigma_{ss} + \sigma_{ll})/2$ and $\epsilon_{sl} = \sqrt{\epsilon_{ss}\epsilon_{ll}}$. This system is subjected to an external asymmetric potential at the center of the box ($z = z_0$) along the z -direction, which is given as

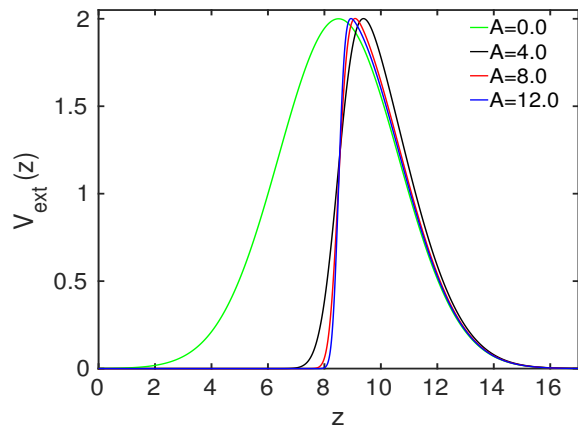


Figure 1. External potential barrier along the z -direction at $z_0 = L/2$ with varying asymmetry parameter $A = 0.0, 4.0, 8.0,$ and 12.0 . Note that $A = 0.0$ is corresponding to the symmetric barrier [23]; the asymmetry in the potential increases with A . On increasing the asymmetry, the position of the potential shifts little to the right, which does not alter dynamics of the system because of the PBCs.

$$V(z) = \epsilon_{ext} e^{-\left(\frac{z-z_0}{\omega}\right)^2} \left[1 + \operatorname{erf} \left\{ A \left(\frac{z-z_0}{\omega} \right) \right\} \right], \quad (2)$$

where ϵ_{ext} , ω , and A are height, width, and asymmetry parameter of the external potential. We have fixed the width $\omega = 3.0$, while varying the ϵ_{ext} and A in this study. The asymmetry parameter $A = 0$ corresponds to the symmetric external potential [24], while non-zero values of A correspond to the asymmetry in the potential. The simulations are carried out by varying the asymmetry parameter as $A = 0-20$, where ϵ_{ext} is adjusted such that the height of the potential remains at 2.0; this potential is plotted in Fig. 1 for few typical values of the asymmetry parameter A . Hereafter, we refer the side of asymmetric potential which coincides with the symmetric Gaussian potential as the *symmetric* side and the one which deviates from symmetric Gaussian potential as *asymmetric* side. We simulate this system at the volume fraction $\phi = 0.2$ and temperatures $T = 2.0-0.3$. The periodic boundary conditions (PBCs) are applied along all the three directions of a cubic simulation box of length $L = 17$; detailed simulation information is given in A. To look at the finite-size effects, we performed simulations of the system at box lengths $L = 15, 19,$ and 21 , keeping other simulation parameters unchanged, which is given in B. Dynamical properties of the system are computed from the phase space trajectories produced in each production run and averaged over five simulation runs, each starting from a random initial configuration.

III. RESULTS AND DISCUSSION

To examine the effect of asymmetry in the barrier on the dynamics of the colloidal mixture, we have calculated mean-squared displacement (MSD) of both sizes of particles along the z -direction as

$$\delta r^2 = \frac{1}{N} \langle (r_z(t) - r_z(0))^2 \rangle. \quad (3)$$

Since the external potential barrier is only along the z -direction and the volume fraction is low, the MSD of both sizes of particles does not show jump or caged like motion at low temperatures along the directions normal to the applied external potential barrier for the symmetric [23] and the asymmetric case (see Fig. A.18 of E). In Fig. 2, we plot the MSD of both species of particles at $T = 1.0$ and $T = 0.3$ at different asymmetry parameters. At the higher temperatures, both the species in the binary mixture undergo normal diffusion at all values of asymmetry parameter A . As expected, the dynamics of the smaller particles is faster than that of the larger particles, as evident from the higher values of MSD for the smaller particles. However, at low temperatures, the MSD of the smaller particles deviates from the linear behavior and develops a plateau at intermediate times. This is due to the localization of the smaller particles between the external potential barriers (multiple barriers arise due to the PBCs), as in the case of symmetric barriers ($A = 0$). However, the MSD of the larger particles remains linear (at long times) even at the lower temperatures due to the attractive depletion interaction between the external potential barrier and the larger particles. The asymmetry in the potential barrier does not affect the qualitative nature of MSD of the smaller particles at all temperatures, though it slows down with A that is pronounced at $A = 10$. This slowing down can be dynamical in the sense that the higher asymmetry in the external potential reduces the probability of larger particles crossing over the barrier, thus have to spend a considerably large amount of time near the barrier. This, in turn, increases the probability of large particles reversing the direction of motion near the asymmetric side, therefore, a probability of finding the smaller particles near the barrier increases. This is evidenced in the peak in density profile of the smaller particles near the asymmetric side of the barrier [see Figs. A.17(a-b)]. This interesting observation will be further investigated. However, the MSD of the larger particles decreases with increasing A . This is expected as the depletion interaction is between the potential barrier and the larger particles and any change in the potential will be mainly affecting the dynamics of the larger particles.

The long time diffusion coefficient of the particles along the direction of external potential barrier in the colloidal mixture is computed as $D_z = \lim_{t \rightarrow \infty} \frac{\delta r^2}{2t}$, where δr^2 is computed from Eq. 3. Figure 3(a) shows a semi-log plot of D_z^s vs the inverse temperature ($1/T$). As temperature decreases, the diffusion coefficient of the smaller particles

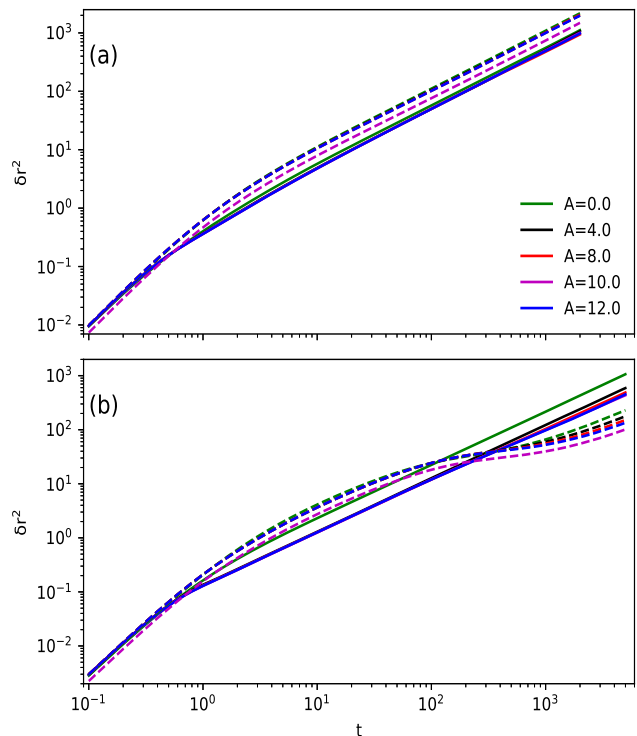


Figure 2. Mean-squared displacement of the smaller (dashed lines) and the larger (solid lines) particles at $A = 0.0, 4.0, 8.0, 10.0,$ and 12.0 . (a) $T = 1.0$ and (b) $T = 0.3$.

decreases rapidly. Here again the asymmetry in the potential barrier does not affect the diffusivity of the smaller particles, except for very large values of A , namely 10 and 12. Here again, diffusion of the smaller particles slows down more at $A = 10$, though it is Arrhenius. The plots are linear and can be fitted with the Arrhenius equation $D = D_0 \exp(-E_a^s/k_B T)$. This essentially means that activation energy for the smaller particles' diffusion is temperature independent. However, the diffusion coefficient of the larger particles decreases rather slowly with temperature, which suggests a non-Arrhenius behavior. As asymmetry in the potential barrier increases, D_z^l starts decreasing faster with decreasing temperature, but the numerical values are still larger compared to D_z^s . The temperature dependence of D_z^l is found to be sub-Arrhenius in the case of symmetric potential barrier [24]. In fact, a general d -Arrhenius equation has been proposed to include the deviations from Arrhenius behavior in diffusion, especially at lower temperatures, as

$$D(T) = A \left[1 - d \frac{E_0}{k_B T} \right]^{1/d}, \quad (4)$$

where E_0 is the height of the barrier and d is the deformation parameter [25]. For $d = 0$, above equation tends to the original Arrhenius equation. For positive values of d , D vs $1/T$ curve will be convex and the behavior is known as the super-Arrhenius diffusion. The most common mechanism known for the super-Arrhenius diffusion

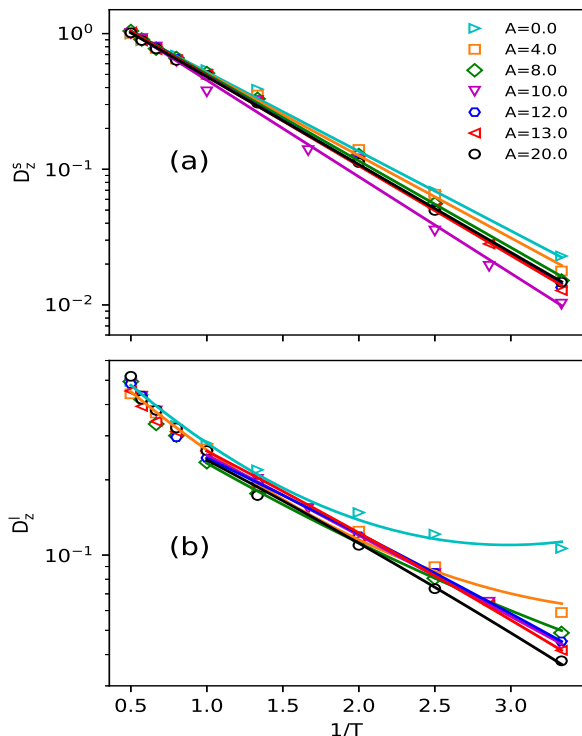


Figure 3. Diffusion coefficient of the (a) smaller particles and the (b) larger particles at temperatures $T = 2.0-0.3$ along the z -direction. Solid lines are fit to the data points, whereas symbols correspond to the data at different asymmetry parameters. At $A = 8.0$ and above, the the diffusion data of the larger particles, is fitted in the temperature range $1.0-0.3$.

is the correlated dynamics of particles such as in the supercooled liquids [32, 33]. For negative values of d , the D vs $1/T$ curve will be concave and the diffusion is said to be sub-Arrhenius. As pointed out in the introduction, the sub-Arrhenius behavior is mostly observed in quantum systems, where quantum tunneling plays a crucial role in the process. From Fig. 3(b), it is clear that the dynamics of the larger particles is sub-Arrhenius at low values of asymmetry in the potential barrier. However, as the asymmetry increases the concave nature of the curve diminishes and become linear or convex. To find this, we have fitted the d -Arrhenius equation and obtained the d values at different values of A , which is shown in Fig. 4. At low values of A , d is negative, a characteristic of the sub-Arrhenius diffusion. However, as A increases, the deformation parameter d increases and for the larger values of A it crosses over to positive values (though small), indicating a crossover from sub-Arrhenius to super-Arrhenius diffusion. On further increasing the asymmetry in the external potential, the d value reached a plateau. This is because the shape of the external potential does not change significantly, at the higher A (see Fig. 1), and the volume fraction of the system is very low. We expect that super-Arrhenius diffusion for the larger particles of the mixture, subjected

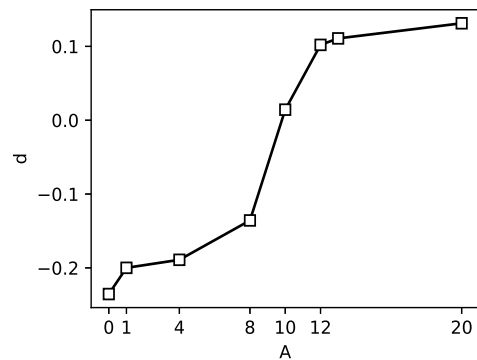


Figure 4. Deformation parameter d is obtained from the fitting of the d -Arrhenius law (Eq. 4) to $\ln(D_z^l)$ vs $1/T$ curves, shown in Fig. 3(b), which is plotted against the asymmetry parameter A .

to the asymmetric external potential barrier, may enhance at the higher system volume fractions, well below ϕ_g . We have calculated the activation energy from the diffusion coefficient of both species of particles by fitting the Arrhenius (for the smaller particles) or d -Arrhenius (for the larger particles) equations from D vs $1/T$ curve; these are plotted in Figs. 5(a-b). The activation energy of the smaller particles shows a little increment with A . Since the diffusion of the larger particles is d -Arrhenius, the activation energy for diffusion is temperature dependent and hence plotted against temperature for different values of A . As temperature decreases the activation energy trend gets reversed for the smaller values of A , however the trend gets reversed for the larger particles at the higher values of A . This is consistent with the change in the sign of d , again suggesting the crossover from sub-Arrhenius to super-Arrhenius diffusion.

To gain further insight into this effect of asymmetry on the diffusive behavior of larger particles, we calculate their density profile, $\rho_l(z)$, along the z -direction. This is plotted in Figs. 6(a-b) for two representative temperatures $T = 1.0$ and $T = 0.3$. The density profile shows peaks in the neighborhood of the external potential barrier on either side. This is due to the attractive depletion interaction between the barrier and the larger particles. For the symmetric barrier ($A = 0$), the peaks are symmetric around the center of the potential barrier, as expected. However, as A increases, the density profile also becomes asymmetric. Moreover, local density increases at the asymmetric side of the potential compared to the symmetric side. For more clarity, this is shown in the left inset of Fig. 6(b). As temperature is lowered, the peak height increases for both peaks of $\rho_l(z)$ at all A . However, the local density at the centre of the potential barrier decreases and approaches close to zero at very low temperatures. To estimate the effective density of particles near and off the barrier, we calculate effective volume fraction along z -direction as $\phi(z) = \frac{\pi}{6L^2 dz} [N_s(z)\sigma_{ss}^3 + N_l(z)\sigma_{ll}^3]$ by slicing the three

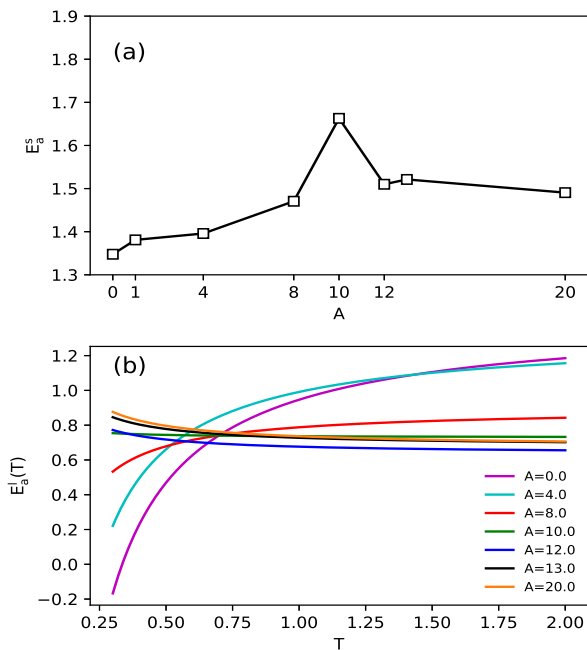


Figure 5. (a) Activation energy of the smaller particles, E_a^s , which is temperature independent, is plotted against A . It shows a least variation with the asymmetry parameter, except at $A = 10$. (b) Activation energy of the larger particles $E_a^l(T)$ is temperature dependent and showing a crossover (from $A = 10$ to above) from sub-Arrhenius to super-Arrhenius diffusion.

dimensional simulation box at width $dz = 0.5$ and calculating number of small (N_s) and large (N_l) particles along z -direction; this is shown in Figs. 7(a-c). The $\phi(z) \simeq \phi (= 0.2)$ at all A away from the barrier, shown at three representative temperatures. However, $\phi(z)$ differs from ϕ near the barrier. It increases equally on both sides of the barrier for $A = 0$ ($\phi^P(z)$ are identical in the insets of Figs. 7(a-c)), which becomes asymmetric with an increasing asymmetry in the potential. This is clearly shown by plotting $\phi^P(z)$ vs A , where the peak height at the symmetric side of the barrier becomes constant from $A = 4$ onwards. On the other hand, the $\phi^P(z)$ at the asymmetric side of the barrier grows faster with A up to $A = 8$, its growth slows down beyond it. Interestingly, at $T = 0.3$, $\phi(z)$ exceeds 0.5 (or $\frac{\phi(z)}{\phi} > 2.5$) beyond $A = 8.0$, approaches $\phi(z) \simeq 0.56$ (at $A = 20$) that is near the glass volume fraction for hard spheres, i.e., $\phi_g = 0.58$ [34]. The crossover from sub-Arrhenius to super-Arrhenius diffusion is also observed beyond $A = 8$ (see Fig. 4). Studies on the role of system density on the kinetic fragility and the configurational entropy show that the kinetic fragility increases whereas the configurational entropy decreases with density, showing a rapid slowing down at the higher densities, one of the key signatures of the supercooled liquids [35, 36]. An accumulation of the particles towards the asymmetric side of the barrier above $A = 8.0$ suggests a frequency of crossing over the barrier decreases with temperature, thus increases local density in the proxim-

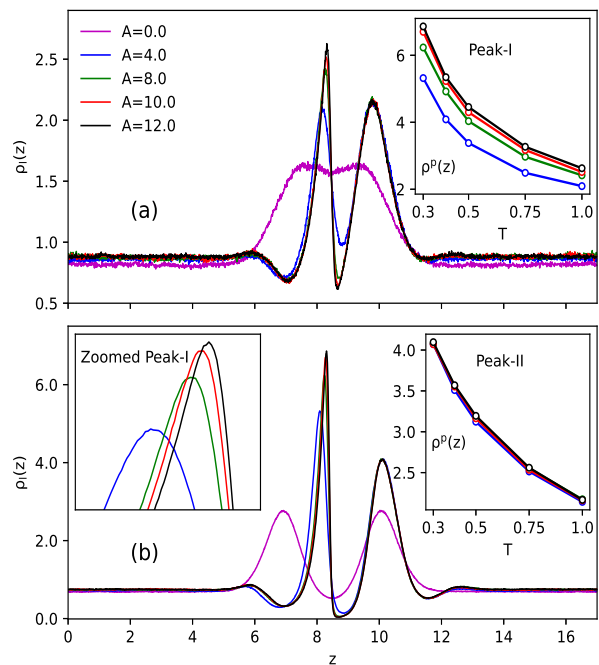


Figure 6. Density profile of the larger particles along the z -direction at $A = 0.0, 4.0, 8.0, 10.0$, and 12.0 . (a) $T = 1.0$ and (b) $T = 0.3$. Top right insets of (a) and (b) show plots of peak heights of $\rho_l(z)$ vs temperature T at $A = 4.0, 8.0, 10.0$, and 12.0 ; these peaks are named as peak I (asymmetric side) and peak II (symmetric side). The zoomed area of the peak I at $T = 0.3$ is shown in the top left inset of (b), showing an increment in its height with position shifting towards right. This signifies an accumulation of the larger particles towards the asymmetric side of the barrier.

ity of the barrier. We calculate potential of mean force for the larger particles, $V_{pmf}^l(z) = -k_B T \ln[\rho_l(z)]$, to examine this depletion effect due to the barrier. Figures 8(a-c) compare $V_{pmf}^l(z)$ of the larger particles at the asymmetry parameters $A = 0.0, 4.0, 8.0, 12.0$ at one higher ($T = 1.0$) and two lower ($T = 0.5, 0.3$) temperatures; $V_{pmf}^l(z)$ varies much with T and A . When the barrier is symmetric, the larger particles are crossing it from both the sides with equal probabilities, even at low temperatures because the height of $V_{pmf}^l(z)$ is nearly zero (more details can be found in Refs. [23, 24]). As A increases, the height as well as the asymmetry in the potential of mean force increases, and the larger particles start accumulating (moreover on the asymmetric side) near the barrier. Since crossing the barrier becomes increasingly difficult for the larger particles at lower temperatures, they aggregate near the barrier on both sides (more on the asymmetric side), which leads to the higher local density of the larger particles. However, there are no signatures of local freezing of layers and crystallization of the particles near the barrier, which is examined by two-dimensional structure factor and shown in Fig. A.16 of C, to keep the continuation of our main results. The smaller particles remain (mostly) away from the barrier, which is due

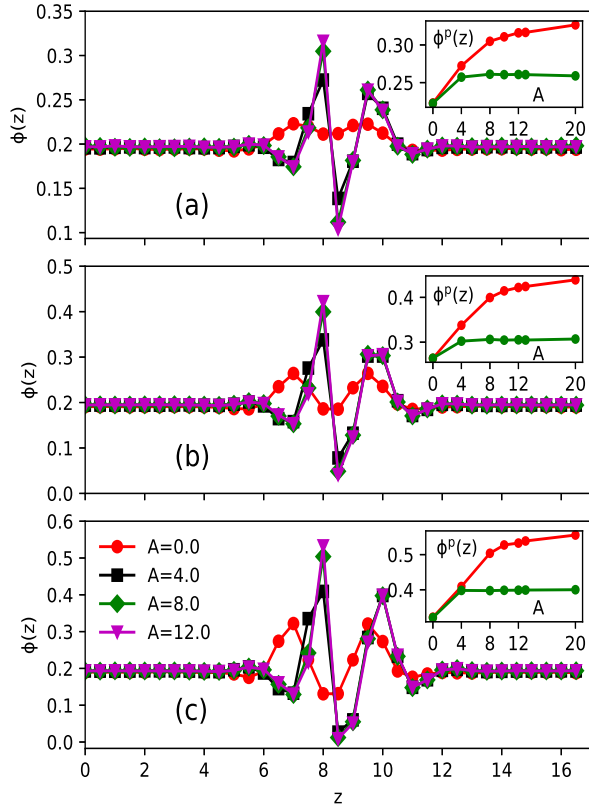


Figure 7. Effective volume fraction of the system (over all particles) along z -direction at asymmetry parameters $A = 0.0, 4.0, 8.0, 12.0$. (a) $T = 1.0$, (b) $T = 0.5$, and (c) $T = 0.3$. Legend of (c) is applied to (a) and (b). Insets of (a-c) show a variation in peak heights of $\phi(z)$, i.e., $\phi^p(z)$, on the asymmetric (red) and symmetric (green) side of the barrier, against the asymmetry parameter A . The increment and constant values of $\phi^p(z)$, at and above $A = 4.0$, on the asymmetric and symmetric side of the barrier, respectively, corroborate with the enhancement of the peaks of $\rho_l(z)$.

to the depletion effect in the binary mixture caused by the symmetric external potential barrier [23, 24]. This in turn leads to local caging and slowing down of the dynamics of the larger particles, which is examined by calculating the non-Gaussian parameter (NGP), the incoherent intermediate scattering function, and the self part of the van-Hove correlation function.

In the case of the symmetric potential barrier, the NGP of the larger particles is (approximately) zero, which indicates that these particles are not localized between the barriers and their dynamics is diffusive even at low temperatures [23]. In contrast to this, the NGP of the smaller particles shows marked deviations from zero at intermediate times as we decrease the temperature. This corresponds to the localization of the smaller particles between the potential barriers resulting in a plateau in MSD at intermediate times [23]. From the MSD's of the smaller particles [see Fig. 2(a)], it is evident that their dynamics does not change qualitatively, though changes quantita-

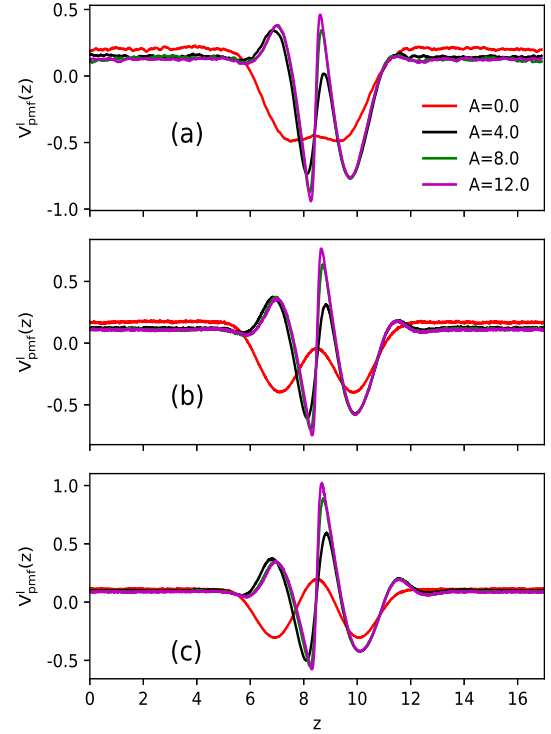


Figure 8. Potential of mean force of the larger particles along z -direction at asymmetry parameters $A = 0.0, 4.0, 8.0, 12.0$. (a) $T = 1.0$, (b) $T = 0.5$, and (c) $T = 0.3$. Legend of (a) is applied to (b) and (c).

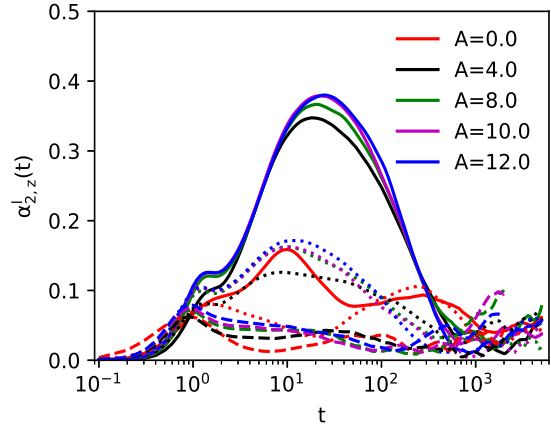


Figure 9. Non-Gaussian parameter of the larger particles along the applied external potential barrier at $A = 0.0, 4.0, 8.0, 10.0, 12.0$, and temperatures $T = 1.0$ (dashed lines), 0.5 (dotted lines), and 0.3 (solid lines).

tively, with A . Therefore, we show the NGP of the larger particles only (see Fig. 9) to examine the cagelike features due to their localization near the barrier, which is

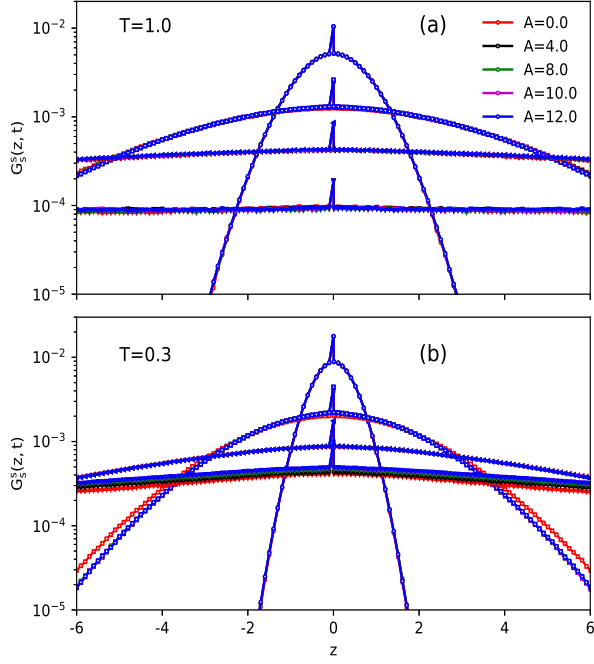


Figure 10. Self part of van-Hove correlation function of the smaller particles at $A = 0.0, 4.0, 8.0, 10.0, 12.0$, and temperatures (a) $T = 1.0$ and (b) $T = 0.3$. The symbols \circ , \square , \triangleleft , and ∇ ($T = 0.3$) correspond to times $t = 1.0, 10.0, 100.0$, and 2000.0 (5000.0).

defined as

$$\alpha_{2,z}^l(t) = \frac{1}{3} \frac{\langle (r_z(t) - r_z(0))^4 \rangle}{\langle (r_z(t) - r_z(0))^2 \rangle^2} - 1.0. \quad (5)$$

Figure 9 shows that NGP of the larger particles is below the value 0.1 at temperature $T = 1.0$, whereas it starts growing from $T = 0.5$ and $A = 4.0$ onwards. Interestingly, from $A = 4.0$ of $T = 0.5$, $\alpha_{2,z}^l(t)$ shows two peaks — first one at time $t \approx 1.0$, while second one at time $t \approx 10.0$ that is shifted towards the longer times at low temperatures and the larger A . At $T = 0.3$, both peaks of NGP grow, which is a clear signature of the onset of the cage-like motion found in supercooled liquids; the time scales of both peaks are akin to the β and α -relaxation time scales in the dynamics of supercooled liquids [37, 38]. Thus, these peaks show the cagelike motion of the larger particles near the barrier, which enhances with the asymmetry parameter A , therefore, the larger particles exhibit super-Arrhenius diffusion at $A = 10.0$ onwards. On contrary, the large particles' NGP does not show any growth up to $A = 1.0$, where sub-Arrhenius diffusion is observed.

The MSD of the larger particles shows sub-Arrhenius diffusion along the z -direction due to crossing of the barrier comprising large jumps over it, which decreases with temperature and asymmetry parameter A . At low temperatures and the larger A , the large particles become caged due to their localization near the external

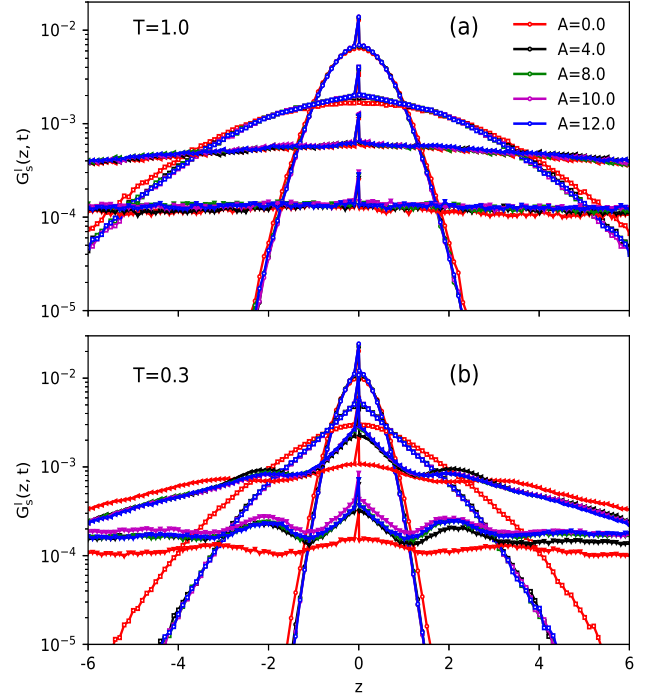


Figure 11. Self part of van-Hove correlation function of the larger particles at $A = 0.0, 1.0, 4.0, 8.0, 10.0$, and temperatures (a) $T = 1.0$ and (b) $T = 0.3$. The symbols \circ , \square , \triangleleft , and ∇ ($T = 0.3$) correspond to times $t = 1.0, 10.0, 100.0$, and 2000.0 (5000.0).

barrier, preferably at the asymmetric side. The cage and the jump like motions together can be examined from the self part of the van-Hove correlation function along z -direction [42], which is defined as

$$G_s(z, t) = \frac{1}{N} \left\langle \sum_{i=1}^N \delta[z - z_i(t) + z_i(0)] \right\rangle. \quad (6)$$

A plot of $G_s(z, t)$ of small particles at $T = 1.0$ and 0.3 is shown in Figs. 10(a–b), showing that $G_s^s(z, t)$ does not depend on the asymmetry parameter at all times; at long times tail of $G_s^s(z, t)$ spreads because the squared displacement increases with time. At low temperatures, e.g., $T = 0.3$, $G_s^s(z, t)$ is independent of the asymmetry parameter A , except at $t = 5000.0$, where it shows a marginal dependency on A . This agrees with the discussion of MSD of the smaller particles, where its trend does not change with A , except at long times where marginal variations are shown. Similar to the smaller particles, $G_s(z, t)$ of the larger particles also does not depend on the asymmetry parameter A at high temperatures (one representative temperature, i.e., $T = 1.0$ is shown) and the shorter time scales, though it changes marginally at long time scales [see Fig. 11(a)]. This is supported from the MSD of the larger particles, and their density profile that does not change much on increasing A at high temperatures — as the peak heights increase marginally

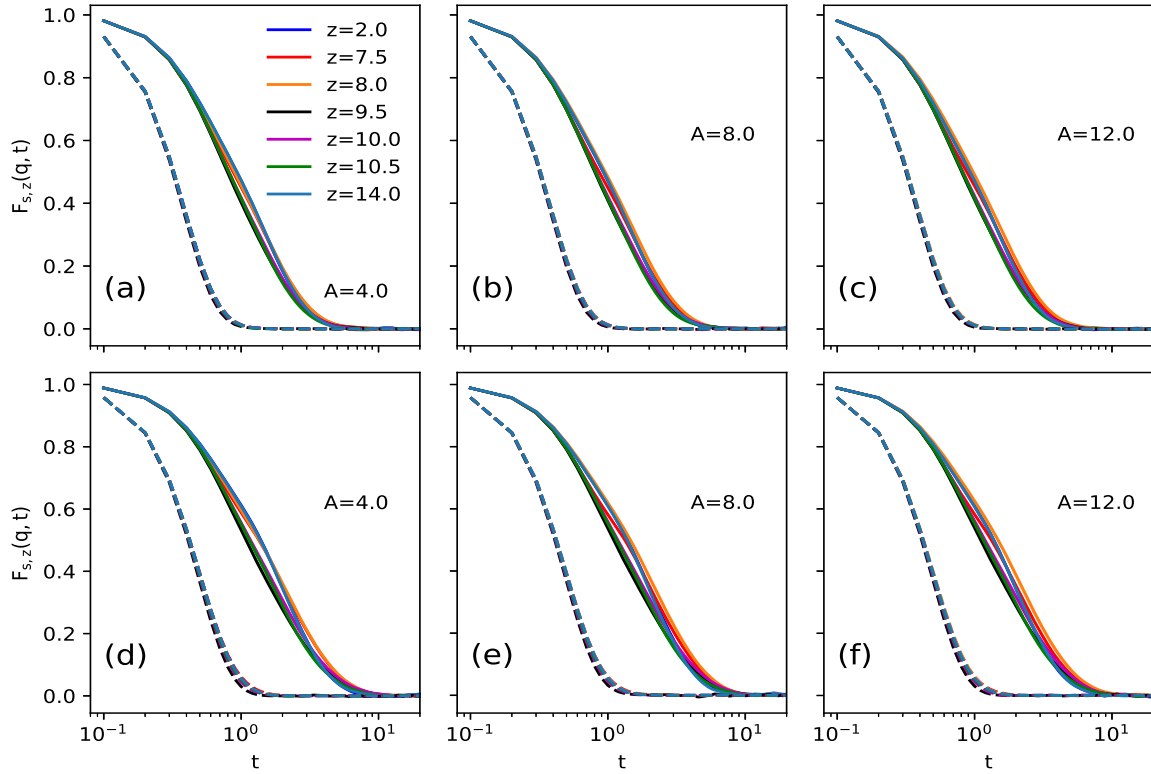


Figure 12. Incoherent intermediate scattering function of the smaller (dashed lines) and the larger (solid lines) particles at low temperatures, $T = 0.5$ (a-c) and $T = 0.3$ (d-f), near and off the barrier, at varying asymmetry. This shows that dynamics of the larger particles is slower than the smaller particles near the barrier. Interestingly, a little hump appears in $F_{s,z}(q, t)$ near the asymmetric side of the barrier, showing their cage like motion.

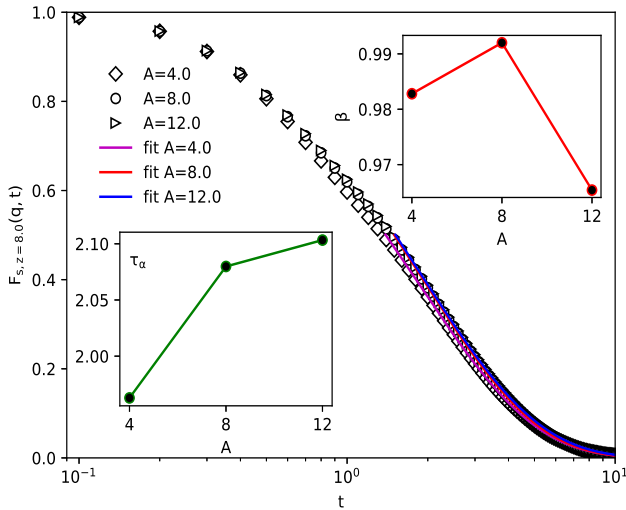


Figure 13. Self intermediate scattering function is plotted against time t at $z = 8.0$ and $T = 0.3$, which is fitted with the empirical Kohlrausch-Williams-Watts (KWW) function of the form $f(t) \propto \exp[-(t/\tau)^\beta]$ [39–41]. The exponent β and the relaxation time τ_α , at $z = 8.0$, are plotted in the top-right and bottom-left insets, respectively.

[see inset of Figs. 6(a–b)]. However, at low temperatures, $G_s^l(z, t)$ varies with the asymmetry parameter A from $t \approx 10.0$, significantly. Interestingly, $G_s^l(z, t)$ start showing a peak from $t \approx 100.0$, which start appearing at $z \simeq 2.0\sigma_U$ for the symmetric potential barrier ($A = 0$), which entails that the larger particles can hop large distances of the order of twice of their diameter. This shows that the larger particles show MSD larger than the expected from $\langle (r_z(t) - r_z(0))^2 \rangle = 2D_z t$, which causes their diffusion to be sub-Arrhenius. The potential of mean force $V_{pmf}(z)$ shows a small effective barrier height ($\epsilon_{ext}^{eff} \simeq 0.2$) at low temperatures of $A = 0$, which means that larger particles can jump over the barrier with a small energy penalty. This peak of $G_s^l(z, t)$ shifts toward the smaller distances with the increment in the asymmetry of the external potential. Interestingly, the peak of $G_s^l(z, t)$ starts approaching toward $z \simeq \sigma_U$ from $A = 4.0$ onwards that reaches at $z \simeq \sigma_U$ for $A = 10.0$, indicating the jumplike motion of the larger particles from the transient cages, similar to one of the characteristics of supercooled liquids. The effective potential barrier height for the larger particles at $T = 0.3$ and $A = 10.0$ is $\epsilon_{ext}^{eff} \simeq 1.0$, which is five times greater than the height at $T = 0.3$ and $A = 0.0$ (symmetric potential). This is a clear signature of the localization at larger A and low

temperatures due to the asymmetric external potential barrier, which alters the diffusion of the larger particles over the barrier from sub-Arrhenius to super-Arrhenius. Interestingly, the oscillating peaks of $G_s^l(z, t)$ are almost identical for positive and negative displacements along the applied potential barrier, indicating the bidirectional transport of the larger particles across it.

Many studies where particles accumulate near a confining wall, show slow relaxation dynamics due to crowding [43–45]. These crowded particles are caged by the surrounding particles, exhibiting slow structural relaxation. It is well established that the self-intermediate scattering function estimates the relaxation dynamics of caged particles. Therefore, the accumulation of particles, in the vicinity of the barrier, is also examined from the (z -dependent) incoherent intermediate scattering function [43], which is calculated as

$$F_{s,z}(q, t) = \frac{1}{N} \left\langle \sum_{i=1}^N e^{-i\mathbf{q} \cdot [\mathbf{r}_i(t) - \mathbf{r}_i(0)]} \delta[z - z_i(0)] \right\rangle. \quad (7)$$

Here, wave numbers $q = 5.4$ and 2.8 are corresponding to peaks of the static structure factor for the smaller and the larger particles, respectively. The $z_i(0)$ is the z -coordinate of an i th particle at time $t = 0$. Figs. 12(a–c) shows that the relaxation dynamics of the smaller particles is almost identical in the sub-Arrhenius ($A < 10$) and the super-Arrhenius ($A > 8$) regimes of the system, near and far from the barrier, even at the lowest temperature ($T = 0.3$) of the study. This is consistent with their mean-squared displacement, diffusion coefficient, van Hove correlation function, and the non-Gaussian parameter. Relaxation dynamics of the larger particles varies with A and the distance from the barrier. In contrast to the smaller particles, the relaxation of $F_{s,z}(q, t)$ of the larger particles is very slow. Interestingly, the relaxation of $F_{s,z}(q, t)$ for the smaller particles is nearly five times faster than the larger particles at both temperatures, shown in Fig. 12. This faster density relaxation of the smaller particles is because it is measured at the wave number associated with the first peak of the static structure factor. This wave number is corresponding to the inter-particle separation. Since the volume fraction is low and the smaller particles are mostly away from the barrier, thus they move faster at the length scale of the inter-particle separation. On contrary, the smaller particles exhibit the slower density relaxation, measured at the length scale of the simulation box ($q = 2\pi/L_z$), as shown by Kumar [23]. Because the smaller particles are trapped between two potential barriers separated by the box length L , due to the periodic boundary conditions. At $T = 0.5$, the dynamics of the larger particles is slower near the barrier compared to far from the barrier. Interestingly, at $T = 0.3$, $F_{s,z}(q, t)$ near the barrier start showing a very little hump, which enhances with increasing asymmetry parameter A . A presence of the hump signifies the cagelike motion of the larger particles near the barrier, which support the behavior of the non-

Gaussian parameter and the self part of the van Hove correlation along the z -direction. For a direct comparison of $F_{s,z}(q, t)$ at $T = 0.3$, we plot it in Fig. 13, at $z = 8.0$ near the asymmetric barrier. We then calculate the α -relaxation time, τ_α and fitted the $F_{s,z=8.0}(q, t)$ with the KWW function to get exponent β . Here τ_α is defined as $F_{s,z}(q, t = \tau_\alpha) = e^{-1}$. Left bottom inset of Fig. 13 shows that τ_α increases (though little) with the asymmetry parameter A . The KWW exponent β is around 0.96 at $A = 12$, which entails the presence of non-exponential density relaxation near the barrier for the larger particles; the tail of $F_{s,z=8.0}(q, t)$ is extended.

IV. SUMMARY AND CONCLUSIONS

We have shown the effect of asymmetry in the external potential barrier along the z -direction, on the structure and dynamics of the binary colloidal mixture using molecular dynamics simulations. Due to the depletion interaction between the potential barrier and the larger particles, the density of the larger particles increases near the barrier. However, as the asymmetry in the potential barrier increases, barrier crossing becomes less probable, leading to even the higher densities near the barrier especially on the asymmetric side. This leads to transient caging of the larger particles. Therefore, for highly asymmetric potential, the diffusion of the larger particles crosses over to super-Arrhenius from sub-Arrhenius diffusion. In general, depletion interactions between the potential barrier and the larger particles makes the activation energy to jump over the barrier, temperature dependent. However, the nature of this dependency changes with the asymmetry parameter in the external potential. At low values of A , the activation energy of the larger particles decreases with temperature, whereas for the larger values of A , it increases with temperature. Thus, the dynamics of the larger particles at very large values of A is very similar to the dynamics of supercooled liquids, where super-Arrhenius diffusion is observed [32, 33, 46]. We expect that at the larger asymmetric potential barrier heights, the super-Arrhenius diffusion will enhance and subsequently the deformation parameter will further increase. This will be interesting since the volume fraction we have used in this study is very low compared to that of supercooled liquids. Moreover, asymmetric potentials are used in the transport of molecules in biological channels [29, 47, 48], targeted delivery of colloids by bacteria [49], and Brownian motors [50, 51]. Most of these studies are carried out for single-component systems in an asymmetric potential subjected to various conditions of driving. It will be interesting to investigate the dynamics of binary mixtures in these scenarios and the system we simulated provides a model for these investigations. Finally, we expect that the experimental realization of our model is straight forward. Spatially asymmetric periodic potentials have been realized in experiments via dielectrophoretically induced forces [52, 53] as well as us-

ing optical tweezers [31]. Dynamics of single-component colloidal systems subjected to an external sinusoidal potential has been studied experimentally by Dalle-Ferrier *et al.* [30]. They have carried out these investigations on two different colloidal systems whose size ratio is close to 1:2, which has been used in our simulations.

ACKNOWLEDGMENTS

The authors acknowledge financial support from the Department of Atomic Energy, India through the 12th plan project (12-R&D-NIS-5.02-0100). The data that support the findings of this study are available from the corresponding author upon reasonable request.

Appendix A: Simulation details

In this equivolume sharing binary mixture at volume fraction $\phi = 0.2$, the number of large and small particles are 117 and 938, respectively at $L = 17$. Thus, the total number of particles in the system are $N = 1055$. The system is simulated in constant NVT ensemble, where the equations of motion, $\dot{\mathbf{q}}_i = \mathbf{p}_i/m$ and $\dot{\mathbf{p}}_i = \mathbf{F}_i - \lambda \mathbf{p}_i$, are simultaneously integrated using the fifth-order Gear predictor-corrector method [42] at the time step of $dt = 0.001$. Here, \mathbf{q}_i , \mathbf{p}_i , and \mathbf{F}_i are position, momentum, and force acting on an i th particle, respectively. The parameter λ is the thermostat factor governed by the Gaussian principle of least constraint [54]. The system is equilibrated at $T = 3.0$ for 1×10^6 steps, then this equilibrated configuration is used as the initial configuration for the rest of the temperatures at the corresponding A . At temperatures $T = 2.0-0.75$, the system is equilibrated till 1×10^6 steps, followed by 4×10^6 production runs. However, at low temperatures, i.e., $T = 0.5$ onwards, the system is equilibrated till 1×10^7 steps, followed by 1.5×10^7 production runs. The equilibration times used in this study are much longer than $100\tau_\alpha$ at all temperatures and asymmetry parameters (see Fig. A.14). To look at the finite-size effects, we simulated the system at box lengths $L = 15, 19$, and 21 , as the equivolume mixtures. The number of particles at these box lengths are $N = 724, 1472$, and 1989 , respectively. Note that the simulation parameters, i.e., time step, equilibration and production runs, etc., are same as the $L = 17$. We used the same simulation procedure for all independent runs and the different box lengths.

Appendix B: Finite-size effects

We calculate the diffusion coefficient of large and small particles at $L = 15, 19$, and 21 , and compare them with the results at $L = 17$, to examine finite-size effects in the system (see Fig. A.15). When the barrier is symmetric, the dynamics is unaffected by changing the box

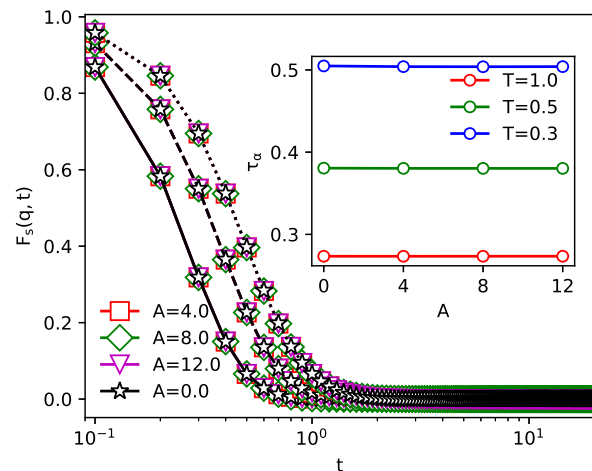


Figure A.14. Incoherent intermediate scattering function, $F_s(q, t) = N^{-1} \langle \sum_{i=1}^N e^{-i \mathbf{q} \cdot \mathbf{r}_i} \rangle$ is plotted against time t . Here, q is the wave number corresponding to the main (first) peak of the static structure factor $S(q)$ and N is the total number of particles in the system. Solid, dashed, and dotted lines are corresponding to $T = 1.0, 0.5$, and 0.3 , respectively. The α -relaxation time increases with lowering temperature, however, it is invariant with A ; at the same temperature, $F_s(q, t)$ coincides for different A . At the lowest temperature, i.e., $T = 0.3$, $\tau_\alpha \simeq 0.5$, and the equilibration time used is $1000\tau_{LJ}$ that is much longer than $100\tau_\alpha$.

lengths, as shown by Mustakim *et al.* [24]. Therefore, we compare diffusion of small and large particles at the symmetry parameters $A = 8.0$ and 12.0 , where the variations in the density profile of the larger particles with A are pronounced [see Figs. 6(a–b)]. Figure A.15 shows that diffusion of the smaller and the larger particles is (approximately) invariant with varying the box length. We change the length of the cubical box and apply external potential at the middle of the z -axis, which adds a periodicity of length L due to the PBCs, therefore, the finite-size effects are unexpected. Thus, the finite-size effects in our simulations of the binary colloidal mixture subjected to the external potential barrier, are insignificant, at the given simulation parameters.

Appendix C: Structure factor

To look at whether the local freezing of the larger particles into layers in xy -plane is taking place along the z -direction, we calculate z -dependent two dimensional (2D) structure factor (near and far from the barrier), which is defined as

$$S(k, z) = \frac{1}{N(z)} \sum_{i,j=1, j \neq i}^{N(z)} \exp[-i \{ \mathbf{k} \cdot (\boldsymbol{\xi}_i(z) - \boldsymbol{\xi}_j(z)) \}], \quad (\text{C1})$$

where $\boldsymbol{\xi}_i(z) = x_i \hat{x} + y_i \hat{y}$, $N(z)$ is the total (small and large) number of particles in a 2D layer at z , and wave

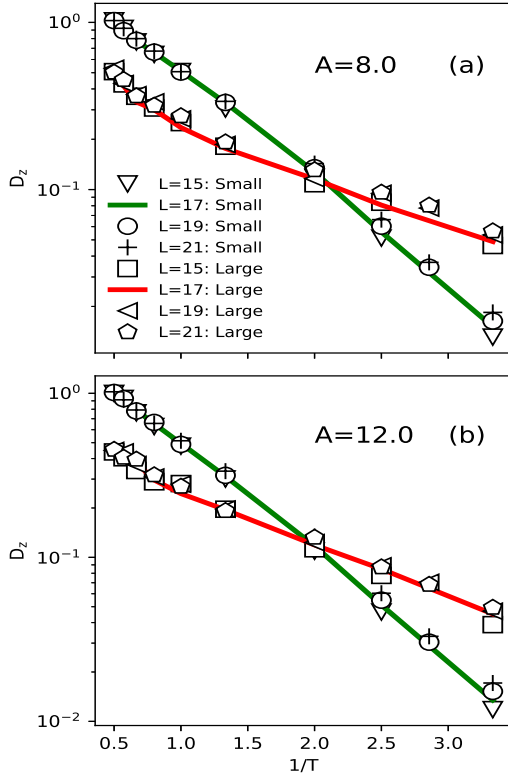


Figure A.15. A comparison of diffusion at four different box lengths, $L = 15, 17, 19,$ and 21 at the asymmetry parameters $A = 8.0$ and 12.0 . The legend of (a) is applied to (b).

vectors are generated in 2D plane. We slice the simulation box along z -direction with a width $dz = 0.5$ to calculate $S(k, z)$, which is shown in Figs. A.16(a-i). $S(k, z)$ is calculated at three representative temperatures, *viz.*, $T = 1.0, 0.5, 0.3$ at asymmetry parameters $A = 4.0, 8.0, 12.0$. At $T = 1.0$ [see Figs. A.16(g-i)], the binary colloidal mixture shows normal liquid structure, as $S(k, z)$ shows a single broad peak at $k \simeq 5$, away from the barrier, and $S(k, z)$ split in to two peaks around $k \simeq 3.0$ and 6.0 , near the barrier. These peaks are corresponding to the two length scales ($k = 2\pi/\sigma_{ss,l}$) due to two different sizes of the particles. At this temperature, $S(k, z)$ slightly differs at different A , specially near the barrier, which is usual because the density profile is different as discussed in the main text. The non-zero values of $S(k, z)$ at low wavenumbers shows the demixing of the particles in the system. At $T = 0.5$ [see Figs. A.16(d-f)], $S(k, z)$ shows pronounced splitting of its main peak near the barrier along with multiple secondary peaks. These peaks are corresponding to the multiple secondary structures near the barrier due to crowding, as seen in the density profile also. At the lowest temperature of the study, *i.e.*, $T =$

0.3 [see Figs. A.16(a-c)], the first peak height of $S(k, z)$ further increases with more splitting in the secondary peak, near the barrier. These secondary peaks are due to multiple secondary structures near the barrier, which is pronounced at low temperatures. Thus, $S(k, z)$ does not show any signature of crystallization of layers near the barrier, although local crowding is present.

Appendix D: Smaller particles' density profile

The dynamics of the smaller particles, discussed in the main paper, shows the anomaly (along z -direction) at the asymmetry parameter $A = 10$. The diffusion coefficient decreases and the activation energy increases at $A = 10$. To examine this, we calculate the density profile of the smaller particles, along the direction of applied external potential at one high ($T = 1.0$) and one low temperature ($T = 0.3$), which is shown in Figs. A.17(a-b). As A increases, (small) peaks in $\rho_s(z)$ develop near the asymmetric side of the barrier, which shows a little attraction of the smaller particles also. However, their number near the barrier is very small compared to the larger particles. This attraction of the smaller particles towards the asymmetric side of the barrier enhances (slightly) at low temperatures and the higher asymmetries. The zoomed peak in the inset of Fig. A.17(b) clearly shows a little increment and shift in the peak near the barrier. Also, a little hump appears towards the symmetric side of the barrier at $T = 0.3$, for $A = 4$ and above. This contrasting nature of $\rho_s(z)$ compared to the symmetric barrier shows that the enhanced activation energy and the smaller diffusion coefficient (at $A = 10$) is because of a very small number of the smaller particles near the barrier. Actually, the number of small particles is very small near the barrier to show any characteristic of the cagelike motion.

Appendix E: Dynamics along X -direction

In a study of the binary colloidal mixture, subjected to symmetric external potential barrier along one of the spatial direction, shows that dynamics of both types of particles along X - and Y -directions is not affected by the barrier [23]. To look at the effect of the asymmetry on the dynamics of the particles in the mixture along one of the directions normal to the z -direction, we plot the MSD's of (both types of) particles at $T = 1.0$ and 0.3 . Figs. A.18(a-b) show that δr_x^2 of the larger particles is invariant with A at $T = 1.0$, however, it slows down slightly at $A \neq 0$ and $T = 0.3$. The smaller particles' MSD along X - direction also shows a little slow down at $A = 10$.

[1] J. C. Crocker, J. A. Matteo, A. D. Dinsmore, and A. G. Yodh, Phys. Rev. Lett. **82**, 4352 (1999).

[2] R. Dickman, P. Attard, and V. Simonian, J. Chem. Phys. **107**, 205 (1997).

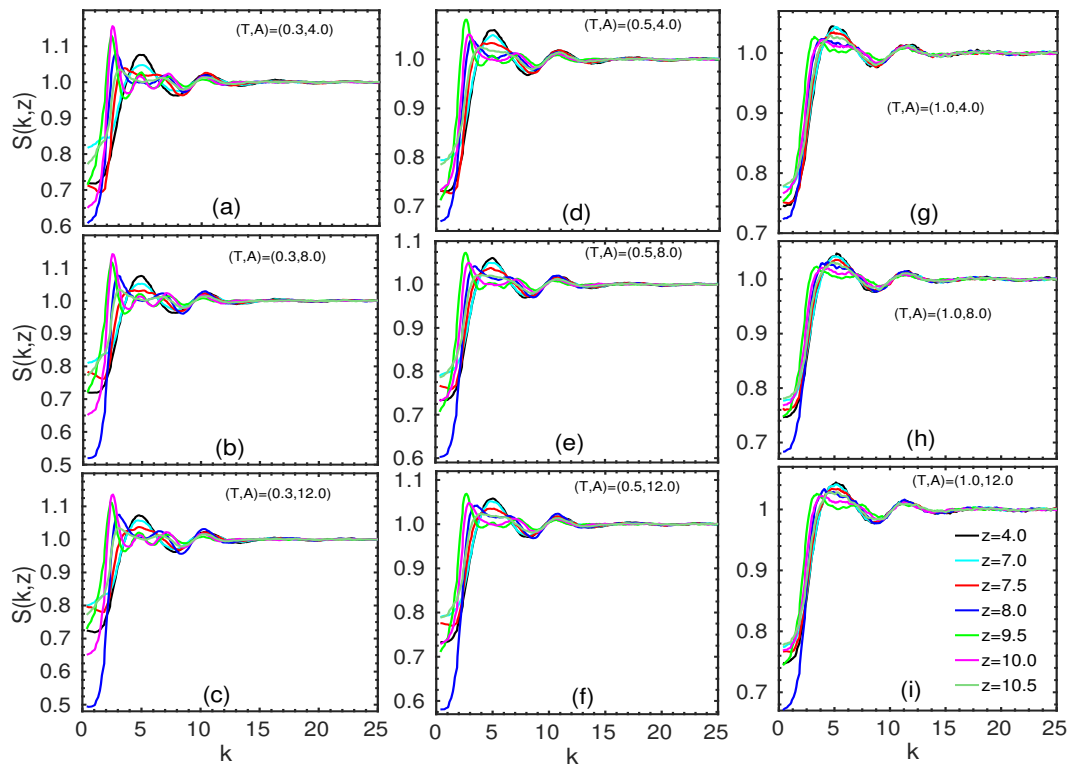


Figure A.16. Two-dimensional structure factor near ($z = 7.0, 7.5, 8.0, 9.5, 10.0, 10.5$) and far ($z = 4.0$) from the external barrier at asymmetry parameter $A = 4.0, 8.0, 12.0$. (a–c) $T = 0.3$, (d–f) $T = 0.5$, and (g–i) $T = 1.0$. Legend of (i) is applied to (a–h).

- [3] P. D. Kaplan, J. L. Rouke, A. G. Yodh, and D. J. Pine, *Phys. Rev. Lett.* **72**, 582 (1994).
- [4] M. D. Eldridge, P. A. Madden, and D. Frenkel, *Nature* **365**, 35 (1993).
- [5] I. E. Igwe, Y. Zong, X. Yang, Z. Ouyang, and K. Chen, *J. Phys. Chem. B* **121**, 5391 (2017).
- [6] H. N. W. Lekkerkerker and R. Tuinier, *Colloids and the Depletion Interaction* (Springer, New York, 2011).
- [7] F. Oosawa and S. Asakura, *J. Chem. Phys.* **22**, 1255 (1954).
- [8] A. Vrij, *Pure Appl. Chem.* **48**, 471 (1976).
- [9] J. C. C. K. Lin, V. Prasad, A. Schofield, D. A. Weitz, T. C. Lubensky, and A. G. Yodh, *Phys. Rev. Lett.* **85**, 1770 (2000).
- [10] A. Kozina, P. Díaz-Leyva, T. Palberg, and E. Bartsch, *Soft Matter* **10**, 9523 (2014).
- [11] H. W. Hatch, W. P. Krekelberg, S. D. Hudson, and V. K. Shen, *J. Chem. Phys.* **144**, 194902 (2016).
- [12] S. M. Oversteegen, C. Vonk, J. E. G. J. Wijnhoven, and H. N. W. Lekkerkerker, *Phys. Rev. E* **71**, 041406 (2005).
- [13] T. Eckert and E. Bartsch, *Phys. Rev. Lett.* **89**, 125701 (2002).
- [14] M. A. Miller, R. Blaak, C. N. Lumb, and J. P. Hansen, *J. Chem. Phys.* **130**, 114507 (2009).
- [15] A. D. Dinsmore, A. G. Yodh, and D. J. Pine, *Phys. Rev. E* **52**, 4045 (1995).
- [16] S. R. Williams and W. van Megen, *Phys. Rev. E* **64**, 041502 (2001).
- [17] P. Germain and S. Amokrane, *Phys. Rev. E* **76**, 031401 (2007).
- [18] N. M. Toan, D. Marenduzzo, P. R. Cook, and C. Micheletti, *Phys. Rev. Lett.* **97**, 178302 (2006).
- [19] R. Tuinier, J. K. G. Dhont, and T.-H. Fan, *Euro. Phys. Lett.* **75**, 929 (2006).
- [20] G. S. Ullmann, K. Ullmann, R. M. Lindner, and G. D. J. Phillies, *J. Phys. Chem.* **89**, 692 (1985).
- [21] A. V. A. Kumar, *J. Chem. Phys.* **138**, 154903 (2013).
- [22] R. Roth, M. Rauscher, and A. J. Archer, *Phys. Rev. E* **80**, 021409 (2009).
- [23] A. V. A. Kumar, *J. Chem. Phys.* **141**, 034904 (2014).
- [24] M. Mustakim and A. V. A. Kumar, *Physica A* **563**, 125462 (2021).
- [25] V. Aquilanti, K. C. Mundim, M. Elango, S. Kleijn, and T. Kasai, *Chem. Phys. Lett.* **498**, 209 (2010).
- [26] V. H. C. Silva, V. Aquilanti, H. C. B. de Oliveira, and K. C. Mundim, *Chem. Phys. Lett.* **590**, 201 (2013).
- [27] I. Kosztin and K. Schulten, *Phys. Rev. Lett.* **93**, 238102 (2004).
- [28] A. B. Kolomeisky, *Phys. Rev. Lett.* **98**, 048105 (2007).
- [29] R. S. Shaw, N. Packard, M. Schröter, and H. L. Swinney, *Proc. Natl. Acad. Sci.* **104**, 9580 (2007).
- [30] C. Dalle-Ferrier, M. Krüger, R. D. L. Hanes, S. Walta, M. C. Jenkins, and S. U. Egelhaaf, *Soft Matter* **7**, 2064 (2011).
- [31] J. J. Thorn, E. A. Schoene, T. Li, and D. A. Steck, *Phys. Rev. Lett.* **100**, 240407 (2008).
- [32] V. K. de Souza and D. J. Wales, *Phys. Rev. B* **74**, 134202 (2006).
- [33] V. K. de Souza and D. J. Wales, *Phys. Rev. Lett.* **96**, 057802 (2006).

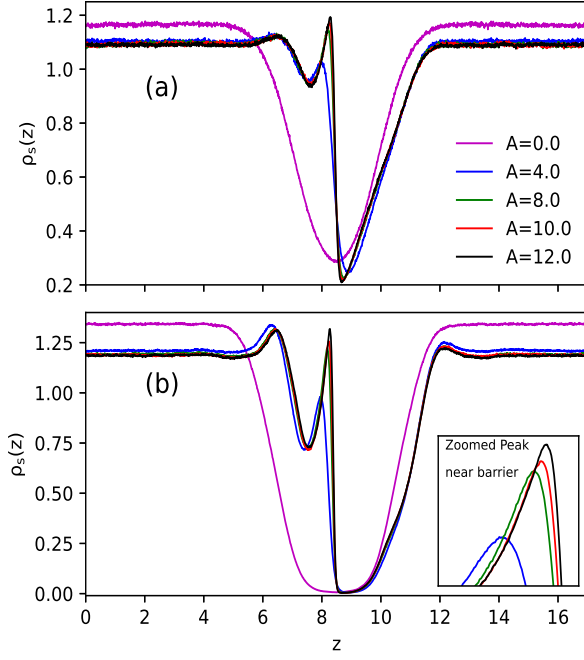


Figure A.17. Density profile of the smaller particles at $A = 0.0, 4.0, 8.0, 10.0,$ and 12.0 . (a) $T = 1.0$ and (b) $T = 0.3$. The zoomed area of the peak, near the barrier at $T = 0.3$, is shown in the inset of (b), showing an increment in its height with position shifting towards right. This signifies a little mixing of the smaller particles towards the asymmetric side of the barrier.

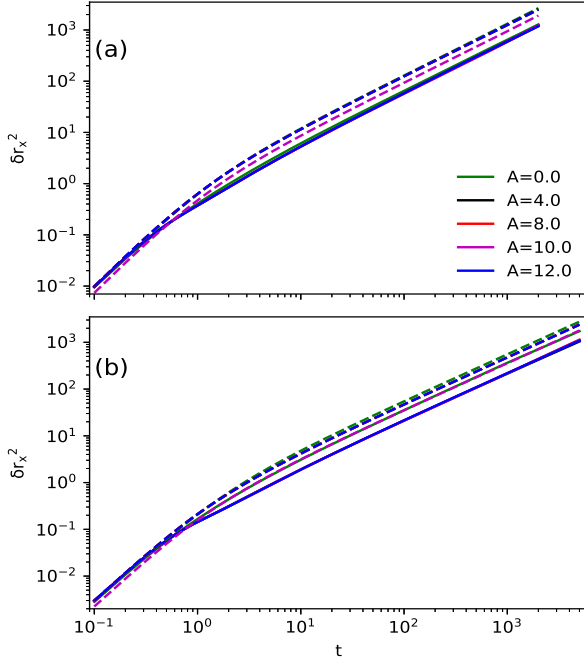


Figure A.18. Mean-squared displacement of the smaller (dashed lines) and the larger (solid lines) particles along X-direction at $A = 0.0, 4.0, 8.0, 10.0,$ and 12.0 . (a) $T = 1.0$ and (b) $T = 0.3$.

- [34] W. van Meegen, T. C. Mortensen, S. R. Williams, and J. Müller, *Phys. Rev. E* **58**, 6073 (1998).
- [35] S. Sastry, *Nature* **409**, 164 (2001).
- [36] S. Sengupta, T. B. Schröder, and S. Sastry, *Eur. Phys. J. E* **36**, 141 (2013).
- [37] L. Berthier, G. Biroli, J.-P. Bouchaud, L. Cipelletti, and W. van Saarloos, eds., *Dynamical Heterogeneities in Glasses, Colloids and Granular Media* (Oxford University Press, Oxford, 2011).
- [38] S. Karmakar, C. Dasgupta, and S. Sastry, *Phys. Rev. Lett.* **116**, 085701 (2016).
- [39] R. Böhmer, K. L. Ngai, C. A. Angell, and D. J. Plazek, *J. Chem. Phys.* **99**, 4201 (1993).
- [40] L. Berthier and G. Biroli, *Rev. Mod. Phys.* **83**, 587 (2011).
- [41] J. Singh and P. P. Jose, *J. Phys.: Condens. Matter* **33**, 055401 (2021).
- [42] J. P. Hansen and I. R. McDonald, *Theory of Simple Liquids* (Academic Press, London, 2006).
- [43] Y.-C. Hu, Y.-W. Li, Y. Yang, P.-F. Guan, H.-Y. Bai, and W.-H. Wang, *Proc. Natl. Acad. Sci.* **115**, 6375 (2018).
- [44] K. Watanabe, T. Kawasaki, and H. Tanaka, *Nature Mater.* **10**, 512 (2011).
- [45] G. M. Hocky, L. Berthier, W. Kob, and D. R. Reichman, *Phys. Rev. E* **89**, 052311 (2014).
- [46] A. Singh and Y. Singh, *Phys. Rev. E* **99**, 030101(R) (2019).
- [47] M. Chinappi, E. D. Angelis, S. Melchionna, C. M. Casciola, S. Succi, and R. Piva, *Phys. Rev. Lett.* **97**, 144509 (2006).
- [48] J. Comelles, D. Caballero, R. Voituriez, V. Hortiguela, V. Wollrab, A. L. Godeau, J. Samitier, E. Martinez, and D. Riveline, *Nature* **107**, 1513 (2014).
- [49] N. Koumakis, A. Lepre, C. Maggi, and R. D. Leonardo, *Nat. Comm.* **4**, 2558 (2013).
- [50] V. M. Rosenbaum, T. Y. Korochkova, A. A. Chernova, and M. L. Dekhtyar, *Phys. Rev. E* **83**, 051120 (2011).
- [51] B. quan Ai and L. gang Liu, *Phys. Rev. E* **76**, 042103 (2007).
- [52] J. Rouselet, L. Salome, A. Ajdari, and J. Prost, *Nature* **370**, 446 (1994).
- [53] L. Gorre-Talini, S. Jeanjean, and P. Silberzan, *Phys. Rev. E* **56**, 2025 (1997).
- [54] D. J. Evans and G. P. Morriss, *Statistical Mechanics of Nonequilibrium Liquids* (Academic Press, London, 1990).